Journal of Biomolecular NMR, **13:** 11–24, 1999.
KLUWER/ESCOM

Solution structure of human acidic fibroblast growth factor and interaction with heparin-derived hexasaccharide

Kenji Ogura[a], Koji Nagata[a], Hideki Hatanaka[a], Hiroko Habuchi[b], Koji Kimata[b], Shin-ichi Tate[c], Mark W. Ravera[d], Michael Jaye[d], J. Schlessinger[e] & Fuyuhiko Inagaki[a,*]
[a]*Department of Molecular Physiology, Tokyo Metropolitan Institute of Medical Science, Tokyo 113-8613, Japan;* [b]*Molecular Medical Laboratory, Aichi Medical School, Aichi 480-1195, Japan;* [c]*Department of Chemistry, Faculty of Science, Tokyo Metropolitan University, Tokyo 192-0397, Japan;* [d]*Rhone-Poulenc Rorer Central Research, PA 19406, U.S.A.;* [e]*Department of Pharmacology, New York University Medical Center, New York, NY 10016, U.S.A.*

Received 26 March 1998; Accepted 9 July 1998

Key words: acidic fibroblast growth factor, ^{1}H, ^{13}C, ^{15}N assignments, heparin binding, secondary structure, triple resonance NMR, three dimensional structure

Abstract

Fibroblast growth factors (FGFs) bind to extracellular matrices, especially heparin-like carbohydrates of heparan-sulfate proteoglycans which stabilize FGFs to protect against inactivation by heat, acid, proteolysis and oxidation. Moreover, binding of FGFs to cell surface proteoglycans promotes to form oligomers, which is essential for receptor oligomerization and activation. In the present study, we determined the solution structure of acidic FGF using a series of triple resonance multi-dimensional NMR experiments and simulated annealing calculations. Furthermore, we prepared the sample complexed with a heparin-derived hexasaccharide which is a minimum unit for aFGF binding. From the chemical shift differences between free aFGF and aFGF-heparin complex, we concluded that the major heparin binding site was located on the regions 110–131 and 17–21. The binding sites are quite similar to those observed for bFGF-heparin hexasaccharide complex, showing that both FGFs recognize heparin-oligosaccharides in a similar manner.

Introduction

Acidic fibroblast growth factor (aFGF) and basic fibroblast growth factor (bFGF) are potent mitogenic polypeptides which play fundamental roles in regulation of cell proliferation, differentiation and promote wound repair and angiogenesis (Burges and Maciag, 1989; Davidson et al., 1985; Gospodarowicz, 1987; McGee et al., 1988; Nabel et al., 1993; O'Keefe et al., 1988; Shipley et al., 1989). FGFs functionally bind to extracellular matrices, especially heparin-like carbohydrates of heparan sulfate proteoglycans (Ruoslahti and Yamaguchi, 1991; Lindhal et al., 1994). Binding to heparin or heparin-like carbohydrates stabilizes FGFs and diminishes inactivation by heat, acid, proteolysis and mild oxidation in vitro (Gospodarowicz and Cheng, 1986; Saksela et al., 1988; Sommer and Rifkin, 1989). Therefore, heparin binding may provide storage and regulated release mechanism for FGFs from cell surfaces (Flaumenhaft et al., 1990). Furthermore, binding of FGFs to cell surface heparan sulfate proteoglycans promotes to form oligomers (Spivak-Kroizman et al., 1994), which is essential for receptor binding and activation (Yayon et al., 1991; Spivak-Kroizman et al., 1994).

Structural studies on free FGFs and the complexes with anti-ulcer agents such as inositol hexasalfate and sucrose octasulfate have been reported (Zhu et al., 1991, 1993; Pineda-Lucena et al., 1994; Moy et al., 1995, 1996; Blaber et al., 1996). Zhu et al. (1991) initially reported the three-dimensional struc-

*To whom correspondence should be addressed.
Supplementary material: A table with assignments for free aFGF (7–140) is available from the corresponding author.

tures of free aFGF and bFGF using X-ray crystallography. Both molecules consist of 12 β-strands, and overall structures form typical β-trefoil structure like IL-1β. Subsequently, Zhu et al. (1993) determined the structure of aFGF complexed with sucrose-octasulfate. While Pineda-Lucena et al. (1994) reported the low resolution solution structure of aFGF complexed with inositol-hexasulfate using ^{1}H-NMR spectroscopy. These studies concluded that drugs bound to a positively charged region of aFGF, largely composed of residues Lys^{112}-Lys^{128}. High-resolution solution structure of bFGF was determined by multi-dimensional heteronuclear magnetic resonance spectroscopy (Moy et al., 1995, 1996), which showed that the solution structure of free bFGF was quite similar to that of the crystalline state. However, there was no apparent β_{XI} strand which was detected in the crystal structure. Most recently, the crystal structures of bFGF complexed with heparin-derived tetra- and hexa-oligosaccharides have been reported (Faham et al., 1996). Heparin formed a helical structure and bound to the residues Asn^{27}, Arg^{120}, Lys^{125}, and Gln^{134} of bFGF. We aligned the sequence of both FGFs based on the structural basis (Figure 1). We also show the residues responsible for heparin binding, receptor binding and central cavity formation in magenta, cyan and green, respectively. Here, we took considerations on the structural studies together with mutagenesis and alanine scanning experiments (Faham et al., 1996; Blaber et al., 1996; Thompson et al., 1994). Most of these residues are well conserved among FGF family proteins, suggesting that FGFs bind to heparin-like oligosaccharides and receptors in a similar manner.

In the present study, we determined the solution structure of free aFGF using multi-dimensional triple resonance NMR spectroscopy. From the analysis of the chemical shift perturbation upon binding of heparin-derived hexasaccharide, we mapped the heparin-binding site on aFGF and discussed the recognition mechanism of heparin by aFGF.

Materials and methods

aFGF preparation

A polypeptide comprising amino acids 7 – 140 of human aFGF was expressed in *Escherichia coli* JM103 bearing the recombinant plasmid pMJ26. Uniformly ^{13}C/^{15}N-labeled aFGF was expressed in M9 medium containing 1 g/L $^{15}NH_4Cl$ and 2 g/L ^{13}C-glucose as nitrogen and carbon sources supplemented with 1 g/L ^{13}C/^{15}N-labeled amino acid mixture from alga (Celltone-CN^{TM};Martek, Columbia, MD). Uniformly ^{15}N-labeled aFGF was also prepared in M9 medium containing 1 g/L $^{15}NH_4Cl$ and 1 g/L ^{15}N-labeled amino acid mixture (Celltone-N^{TM}), while unlabeled aFGF was expressed in LB medium. The lysate was applied to heparin-Sepharose (Pharmacia, Uppsala) column. aFGF was eluted at 1.5 M NaCl concentration and was further purified as described previously (Jaye et al., 1987; Tate et al., 1992). To the sample solution of aFGF, $(NH_4)_2SO_4$ was added to a concentration of 100 mM, which prevented the protein from precipitation.

NMR sample preparation

The NMR sample solution was concentrated and solvent-exchanged by a Centriprep 10 (Amicon, Beverly, MA) concentrator and was finally prepared in 100 mM $(NH_4)_2SO_4$ and 25 mM sodium phosphate buffer in 90% H_2O/10% $^{2}H_2O$ containing 1.5 mM aFGF. Sample volume was 230 μL in a restricted-volume Shigemi NMR tube (Shigemi, Tokyo). The pH of the protein solutions was adjusted to 6.6 by adding 0.1 N HCl or NaOH solution. pH meter readings were not corrected for isotope effects.

Heparin-derived hexasaccharide preparation

Heparin oligosaccharides were prepared by partial deaminative cleavage of heparin as described previously (Thunberg et al., 1982). These oligosaccharides were subjected to a column of Sephadex G-50 (1.2 × 127 cm) equilibrated with 0.2 M ammonium acetate. The hexasaccharide fraction was pooled and purified by chromatography on the same column. The fraction was applied to a column of aFGF-conjugated Sepharose (16 × 35 mm, 7 mL), which had been prepared as described previously (Habuchi et al., 1992) and equilibrated with 10 mM Tris HCl, pH 7.2 and 5 mM dithiothreitol (Solution A) containing 0.15 M NaCl at 4 °C. The column was washed with 35 mL of solution A containing 0.2 M NaCl and then eluted with 28 mL of Solution A containing 1.5 M NaCl. The eluate was desalted using PD 10 column (Pharmacia, Uppsala). The compositional analysis of the bound hexasaccharide was performed as described previously (Habuchi et al., 1992; Bienkowski and Conrad, 1985).

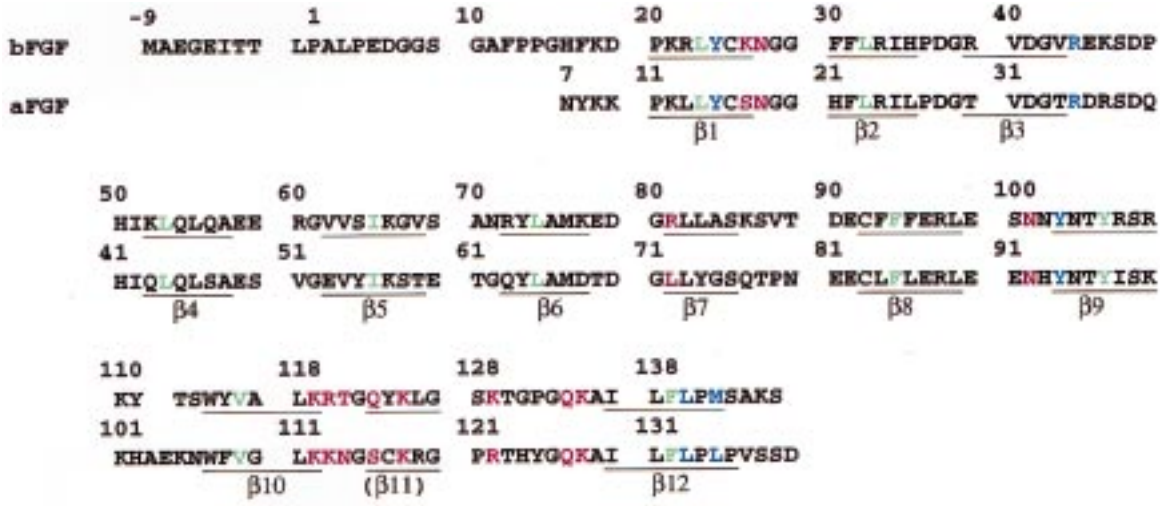

Figure 1. Sequence alignment of basic FGF and acidic FGF on the structural basis. Residues responsible for heparin binding, receptor binding and cavity formation are shown in magenta, cyan and green, respectively.

NMR spectroscopy

All NMR experiments were performed at 30 °C on a Varian UNITY 500 NMR spectrometer equipped with a triple resonance 5 mm probe with a self-shielded z-axis gradient coil. Since we used a single sample dissolved in 90% H_2O/10% ^2H_2O for all NMR experiments, efficient water suppression was essential and we incorporated several water suppression schemes in the pulse sequences as described in the followings.

For homonuclear two-dimensional experiments, water suppression was achieved using the solvent presaturation pulses during the relaxation delay, while water signal in heteronuclear experiments was suppressed either with a combination of presaturation pulses during the relaxation delay and pulsed field gradients as a zz-filter (Bax and Pochapsky, 1992) or with the gradient enhanced HSQC pulse scheme (Kay et al., 1992).

Homonuclear two-dimensional DQF-COSY and TOCSY (Cavanagh et al., 1996) experiments were acquired on unlabeled aFGF dissolved in H_2O solution. In order to observe the aromatic proton signals with suppression of the overlapping amide proton signals in ^{15}N-labeled protein, we measured the ^{15}N-filtered NOESY spectrum (Ogura et al., 1996a).

Two-dimensional ^{1}H-^{15}N HSQC spectrum was acquired on the uniformly ^{15}N-labeled protein. Two-dimensional ^{1}H-^{13}C CT-HSQC (Cavanagh et al., 1996) spectra of the uniformly ^{13}C/^{15}N-labeled protein were acquired.

The following three-dimensional spectra were acquired; HNCO, HNCA, HN(CO)CA, CBCANH, CBCA(CO)NH, HN(CA)HA, HBHA(CO)NH, C(CO)-NH, H(CCO)NH and HCCH-TOCSY (Cavanagh et al., 1996). For ^{13}C isotropic mixing in the HCCH-TOCSY, C(CO)NH and H(CCO)NH experiments, 18 ms DIPSI-3 pulse sequences (Shaka et al., 1988) were employed.

Three-dimensional ^{13}C-edited NOESY (Cavanagh et al., 1996) spectrum of uniformly ^{13}C/^{15}N-labeled protein was acquired as described previously by Ogura et al. (1996b) with a mixing time of 80 ms. Three-dimensional ^{15}N-edited NOESY (Cavanagh et al., 1996) spectrum was acquired on uniformly ^{13}C/^{15}N labeled protein with a mixing time of 80 ms. Three-dimensional HNHA (Vuister and Bax, 1993) spectrum was acquired on uniformly ^{15}N labeled protein. In Table 1, we summarized acquisition parameters for the present NMR experiments.

Acquired homonuclear two-dimensional FID data were processed with a standard VNMR (Varian Instruments, Palo Alto, CA) software package. Other heteronuclear and three-dimensional FID data were Fourier-transformed with the NMRPipe (Delaglio et al., 1995) software package on a SUN SPARC Station 20 computer. The transformed spectra were converted to FELIX 95.0 (Molecular Simulations, San Diego, CA) format with an in-house format-converting software. The resonances were picked using an in-house shoulder peak picking program (Hatanaka et al., unpublished) on the FELIX 95.0 format. Spectral brows-

Table 1. Experiments for free aFGF resonance assignments and structure calculation

Experiment	Carrier (^{13}C, ppm)	Carrier (^{15}N, ppm)	sw (F_1, ppm)	sw (F_2, ppm)	np (t_1)	np (t_2)	Scans	Time (h)
2D DQF-COSY			14.0		512		32	20
2D TOCSY			14.0		400		16	8
2D ^{15}N filtered NOESY		117.7	14.0		512		32	20
2D ^{1}H-^{15}N HSQC		117.7	36		256		4	0.6
3D HNCO	177.1	117.7	13.5	36	50	32	8	16
3D HN(CO)CA	55.3	117.7	28.7	36	64	32	8	20
3D HNCA	55.3	117.7	28.7	36	64	32	8	20
3D CBCA(CO)NH	41.0	117.7	70.0	36	58	32	16	36
3D CBCANH	41.0	117.7	70.0	36	58	32	32	71
3D HN(CA)HA	55.3	117.7	4.0	36	36	32	16	22
3D HBHA(CO)NH	41.0	117.7	7.0	36	64	32	16	38
3D C(CO)NH	41.0	117.7	70.0	36	64	32	32	72
3D H(CCO)NH	41.0	117.7	7.0	36	64	32	32	72
3D HCCH-TOCSY	41.0		7.0	23.3	150	32	8	47
2D ^{1}H-^{13}C CT-HSQC$_{aliphatic}$	41.0		70.0		200		32	4
2D ^{1}H-^{13}C CT-HSQC$_{aromatic}$	124.0		31.8		50		64	2
3D ^{15}N-edited NOESY		117.7	14.0	36	150	32	8	51
3D ^{13}C-edited NOESY	75.2		14.0	48	128	32	8	43
3D HNHA		117.7	9.0	36	64	32	32	79

sw: spectral width; np: number of points (complex); time: total measuring time.

Table 2. Structural statistics

Parameter	<SA>	<SA>$_r$
Rmsd from experimental distance constraints (Å) (1368)	0.025 ± 0.001	0.023
Number of distance constraint violations greater than 0.5 Å	0 (max. 0.42)	0 (max. 0.27)
Rmsd from experimental dihedral constraints (deg) (51)	0.13 ± 0.24	0
Number of dihedral constraint violations greater than 5.0 deg	0 (max. 4.6)	0 (max. 0.5)
F_{NOE} (kcal/mol)	42.1 ± 2.9	35.4
F_{cdih} (kcal/mol)	0.03 ± 0.08	0
F_{repel} (kcal/mol)	25.0 ± 2.7	19.9
E_{L-J} (kcal/mol)	-350.8 ± 49.7	-223.1
Rmsd from idealized geometry		
Bonds (Å) (2148)	0.003 ± 0.000	0.002
Angle (deg) (3875)	0.613 ± 0.009	0.567
Improp (deg) (1128)	0.453 ± 0.023	0.37

<SA> refers to the final set of simulated annealing structures, and <SA>$_r$ is the mean structure. The number of terms is given in parentheses. The value of the square-well NOE potential, F_{NOE}, is calculated with a force constant of 50 kcal/mol per Å^2. The value of F_{cdih} is calculated with a force constant of 50 kcal/mol per rad^2. The value of F_{repel} is calculated with a force constant of 4 kcal/mol per Å^2 with the van der Waals radii scaled by a factor of 0.8 of the standard values used in the CHARMm empirical function.

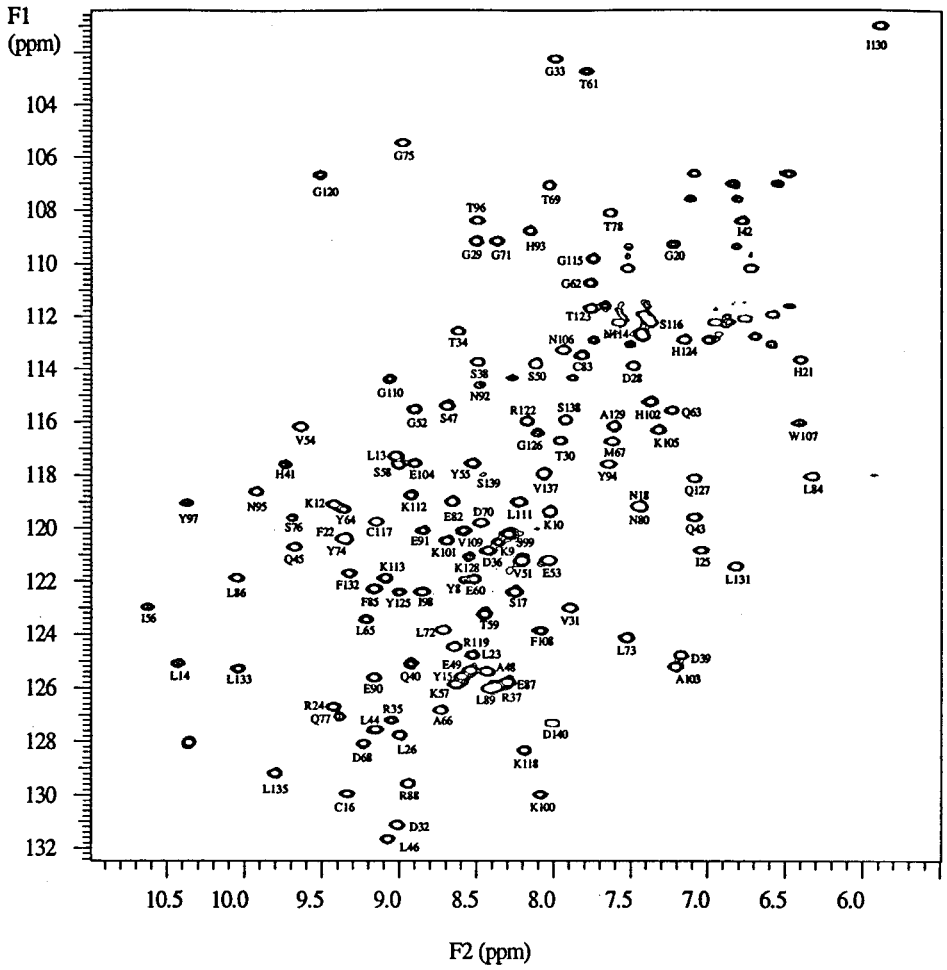

Figure 2. ^{1}H-^{15}N HSQC spectrum of 1.5 mM uniformly ^{15}N-labeled free aFGF. The spectrum was acquired at 500 MHz with four scans and 256 complex points in t1 were acquired. The correlation peaks derived from the backbone amide protons and amide nitrogens are assigned.

ing was carried out with the FELIX 95.0 software on the SUN SPARC Station 20 computer.

Structure calculations

Structure calculations for free aFGF were made after the method of Hatanaka et al. (1994) on a Silicon Graphics Indigo^2 Extreme computer. Interproton distance constraints were derived from NOE cross peak intensities (peak height) in the NOESY spectra. The peak intensities were translated into distance constraints based on the relation of NOE intensity $\propto$ (distance)$^{-6}$ and a standard distance of sequential $d_{\alpha N}$ in β-sheet = 2.2 Å (Wüthrich, 1986). The three-dimensional structures were calculated with XPLOR v. 3.1 (Brünger, 1993) using YASAP. The final 20 converged structures were selected from 200 runs of calculations on the basis of agreement with the experimental data. A mean structure was obtained by averaging the coordinates of the structures that were superimposed in advance on the best converged structure and then minimized under the constraints.

Analysis of the calculated structures

For quantitative assessment of the convergence of the calculations, root-mean-square (rms), number of NOE violations, and the values of F_{repel}, F_{NOE}, and F_{cdih} were examined. An NOE violation is defined as a deviation of the calculated interproton distance from the experimental distance constraint. For quantitative comparisons of the different structures, minimum rms distances (rmsd) were calculated for the specified atoms for all the residues. A mean structure was ob-

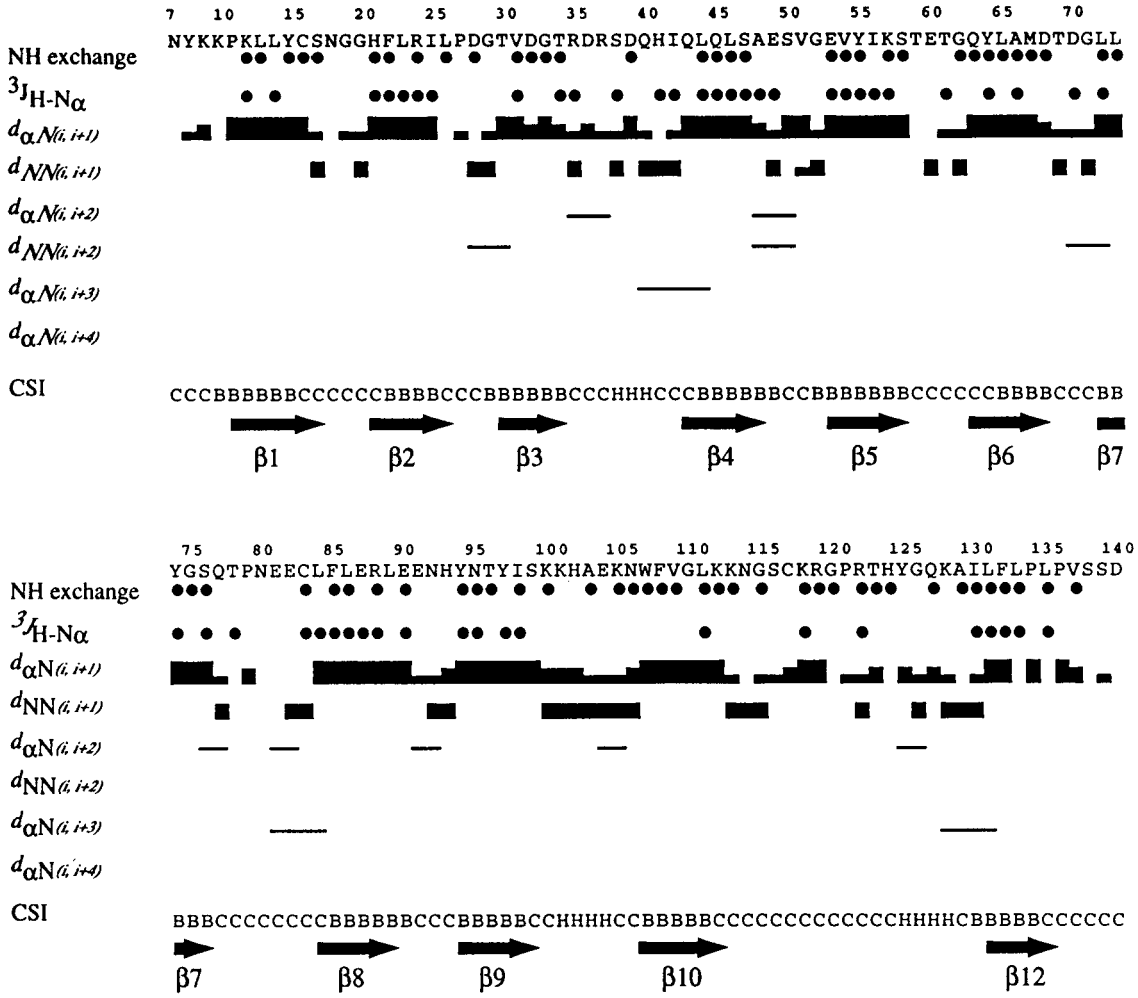

Figure 3. Diagram of sequential and short-range NOE connectivities, hydrogen exchange rates, coupling constant data, and consensus CSI for free aFGF. The NOE correlations were determined from a 3D ^{15}N-edited NOESY spectrum at 30 °C. The height of the bar indicates the strength of the NOE correlation. Filled circles at NH exchange indicate slowly exchangeable amide protons estimated from the water-exchange peak intensity of the 3D ^{15}N-edited NOESY spectrum. Filled circles at the $^{3}J_{H}N_{H}\alpha$ indicate large (> 8 Hz) coupling constants calculated from the ratio of peak intensities of the 3D HNHA spectrum, respectively. Characters B, C and H at CSI indicate the stranded, coiled and helical structures estimated from the consensus CSI of C^{α}, C^{β}, C′ and H^{α} chemical shift values, respectively.

tained by averaging the coordinates of the structures that were superimposed to the best converged structure with a minimum pairwise rmsd of the backbone atoms (N, C^{α}, C′).

Results and discussion

aFGF is thermolabile and is precipitated even at room temperature. But in the presence of 100 mM $(NH_4)_2SO_4$, aFGF was found to be stable and provided a high quality of NMR spectrum as revealed in the ^{1}H-^{15}N HSQC spectrum (Figure 2). Thus, 1.5 mM aFGF sample dissolved in 100 mM $(NH_4)_2SO_4$ and 25 mM sodium phosphate buffer (90% H_2O/10% $^{2}H_2O$) was used for all NMR measurements. We carefully designed the pulse sequences to optimize the efficiency of water suppression so that we could measure all the spectra in 90% H_2O/10% $^{2}H_2O$ solution.

Assignments of resonances

The sequential resonance assignments of free aFGF were achieved based on the analysis of a suite of the HNCA, HN(CO)CA, CBCANH and CBCA(CO)NH spectra. All the main-chain resonances were assigned

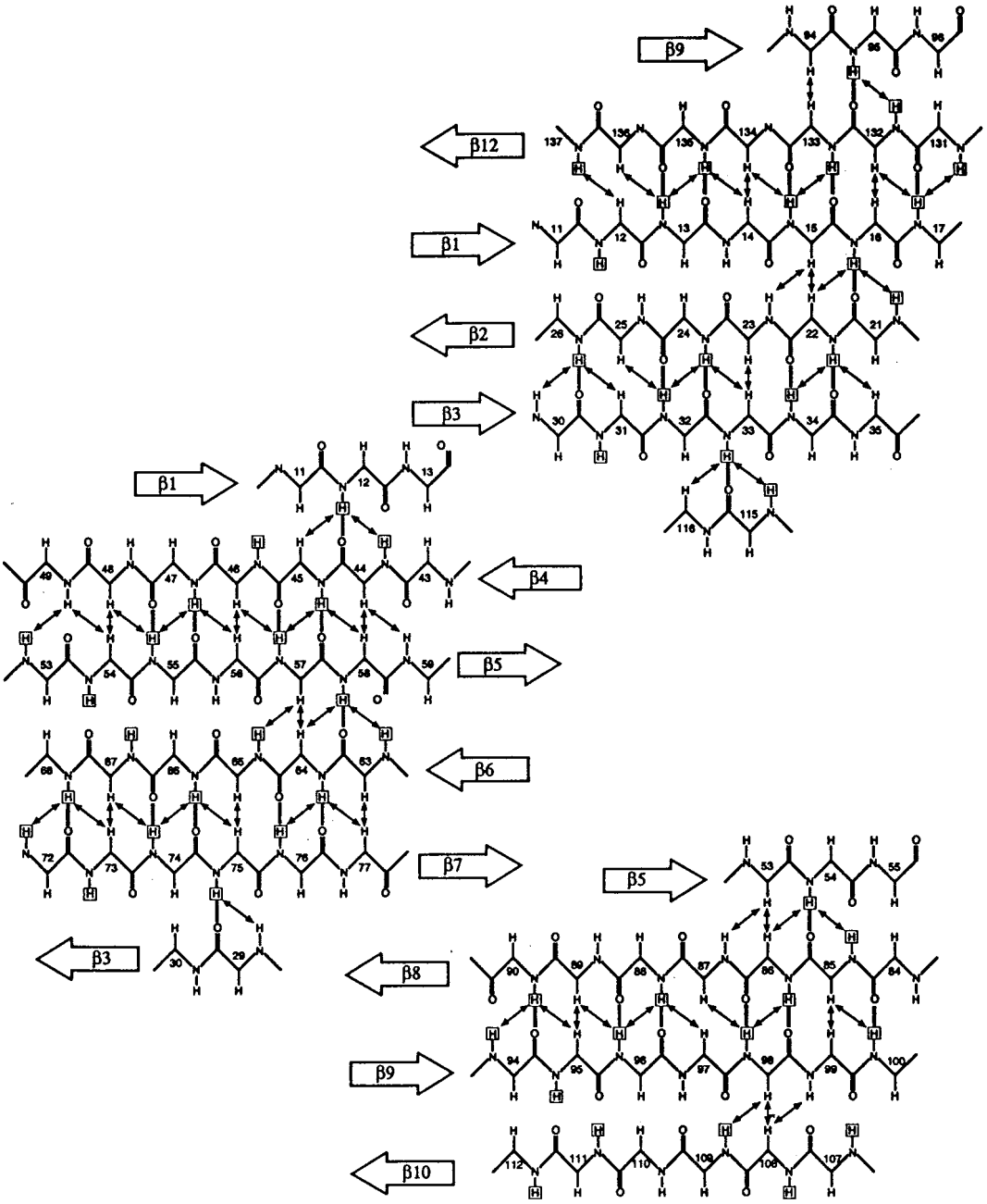

Figure 4. Schematic drawing of the secondary structure and β-sheet topology of free aFGF obtained from the inter-strands H^N-H^N, H^N-H^α and H^α-H^α correlations observed in 3D ^{15}N-edited and ^{13}C-edited NOESY spectra. An open square indicates a slowly exchangeable amide proton. Gray bars represent hydrogen bonds derived from hydrogen exchange rates and NOE patterns.

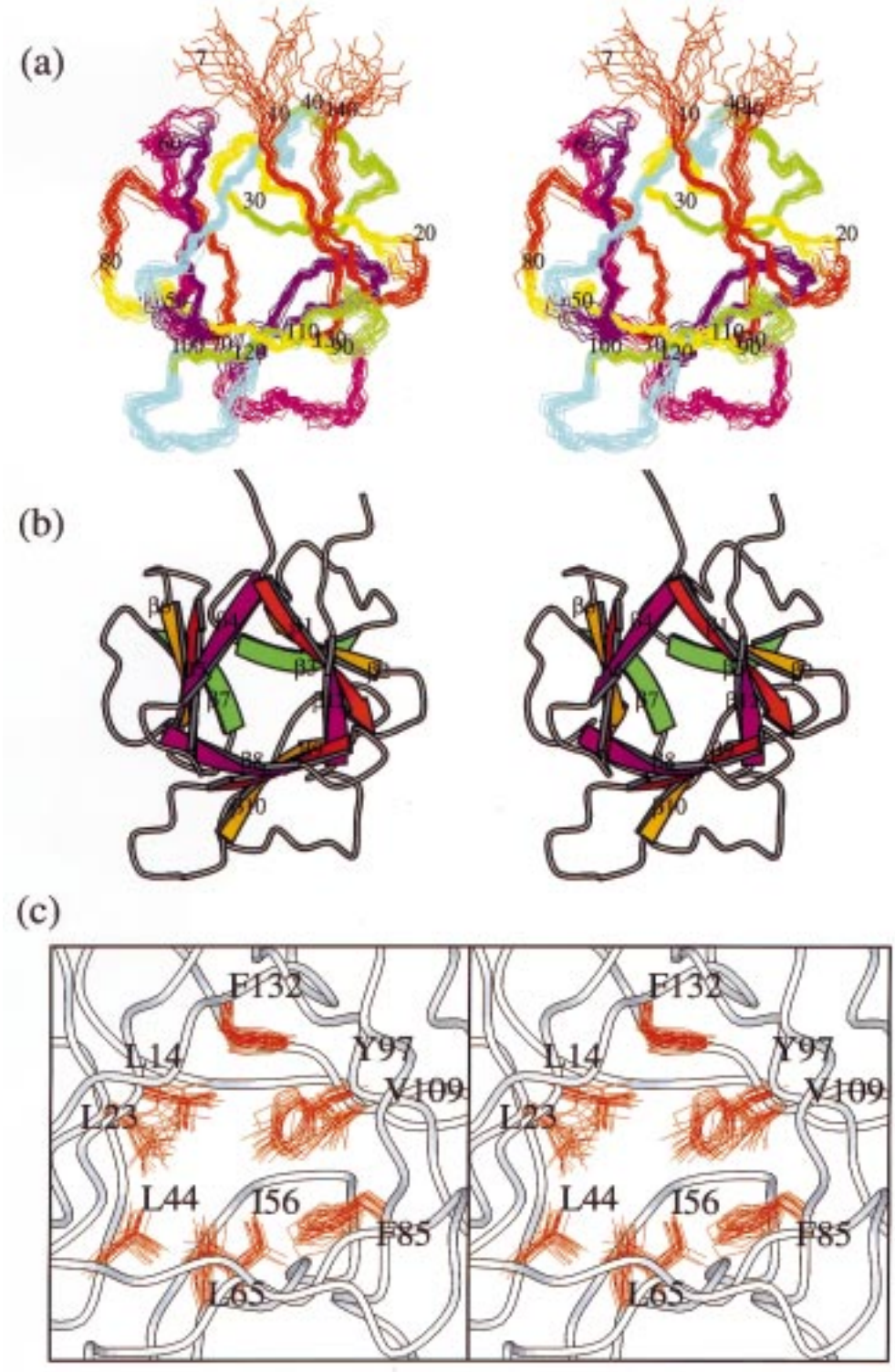

Figure 5. Stereo drawings of tertiary structures of free aFGF. (a) Best-fit superposition of the backbone (N, C^{α} and C′) atoms of the 20 final solution structures of free aFGF. Color changes in every 10 residues; Red (7–20 and 70–80), yellow (20–30 and 80–90), green (30–40 and 90–100), cyan (40–50 and 110–120), blue (50–60 and 120–130), and purple (60–70 and 130–140). (b) Ribbon diagram of the mean structure of free aFGF. The 11 β-strands are colored in red (β_I, β_V and β_{IX}), brown (β_{II}, β_{VI} and β_X), green (β_{III}, β_{VII} and β_{XII}) and violet (βI_V and β_{VIII}). Both figures were produced by the program MOLSCRIPT (Kraulis, 1991). (c) The central cavity and its surrounding residues of aFGF. An overlay of 20 side-chain structures for Phe^{132}, Leu^{14}, Leu^{23}, Leu^{44}, Ile^{56}, Leu^{65}, Phe^{85}, Tyr^{97} and Val^{109} is plotted on the main chain of the mean structure of aFGF.

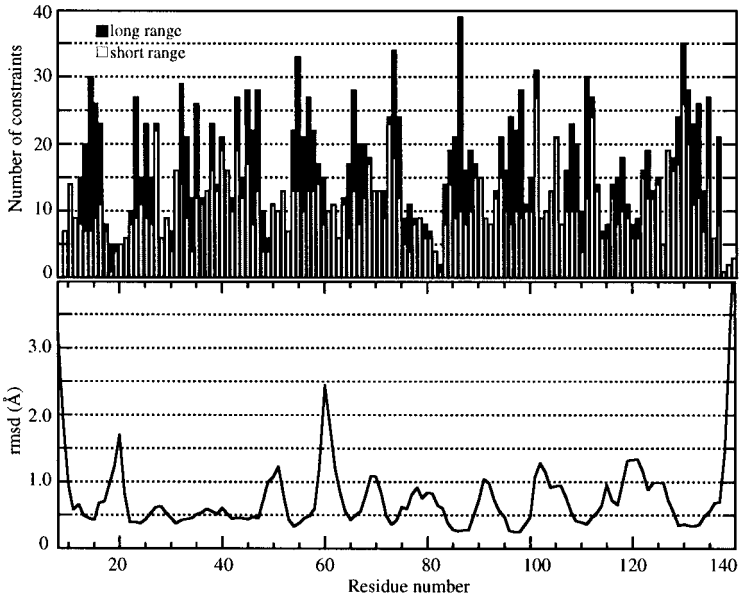

Figure 6. Number of NOE constraints (upper) and rmsd values (lower) for each residue. The numbers of long range ($|i - j| > 5$) and short range ($|i - j| \leq 5$) distance constraints were plotted by black and gray bars respectively as a function of residue number. The average value of the 20 main chain (N, C^{α}, C′) rmsd from the minimized mean structure were also plotted as a function of residue number.

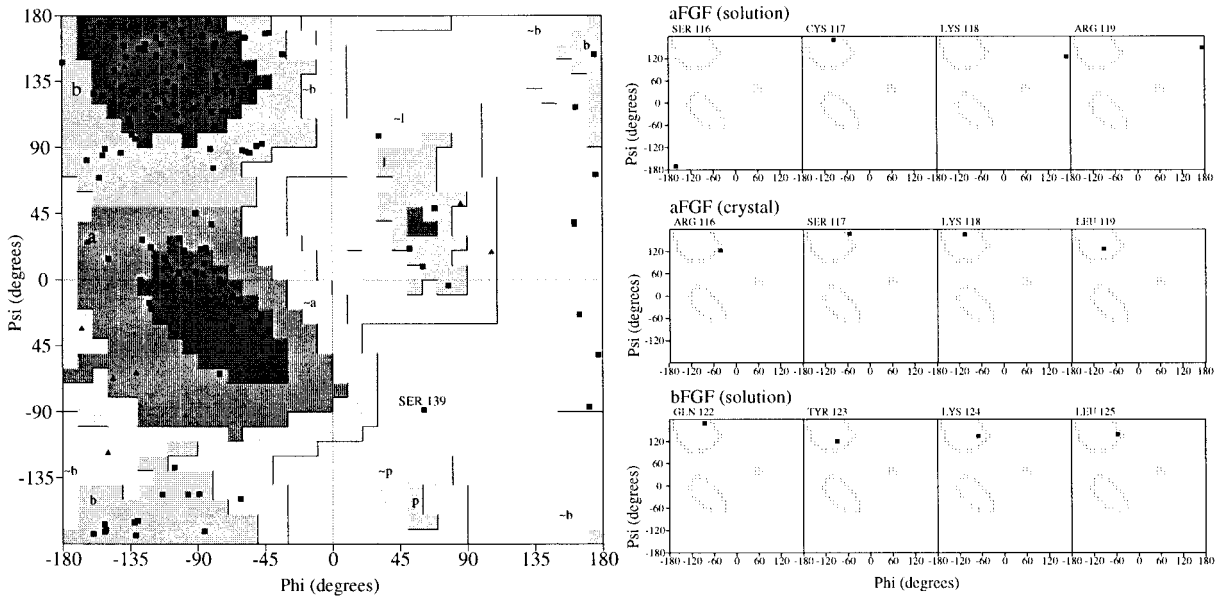

Figure 7. (Left) Ramachandran plot for all residues of the minimized averaged structure of aFGF. (Right) Ramachandran plot for four residues in the β_{XI} region of three FGF molecules (solution and X-ray structure of aFGF and solution structure of bFGF). The figures were produced with the program PROCHECK-NMR (Laskowski et al., 1996).

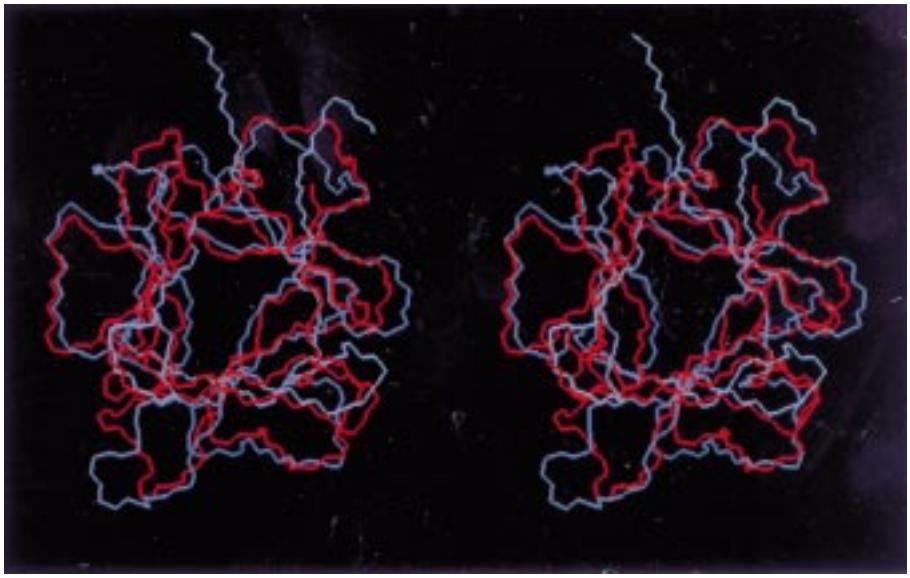

Figure 8. Stereo view of an overlay plot for the X-ray (red) and the solution structure (blue) of aFGF. The main-chain (H^N, C^α, and C') atoms are displayed. The figure was produced with QUANTA (Molecular Simulations, San Diego, CA).

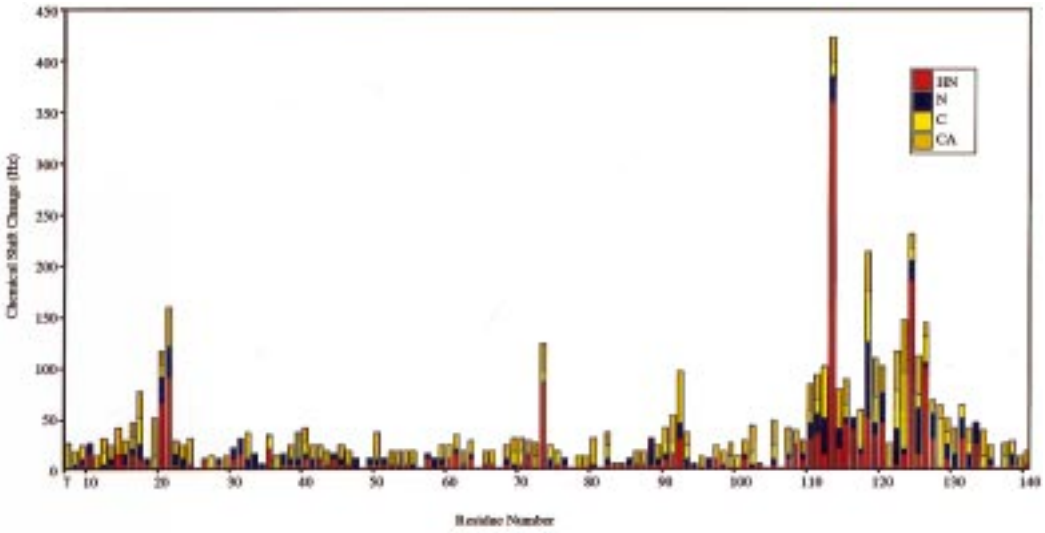

Figure 9. Hep6-induced chemical shift changes of the backbone amide hydrogen ($^1H^N$), nitrogen (^{15}N), α-carbon ($^{13}C^\alpha$), and carbonyl carbon ($^{13}C'$) atoms of aFGF. The absolute values of the chemical shift differences for H^N (red), N (blue), C^α (yellow) and C' (orange) atoms between the complex of $^{13}C/^{15}N$-labeled aFGF:Hep6 (1:1.2 ratio) and free $^{13}C/^{15}N$-labeled aFGF are plotted in Hz unit.

except for N-terminal Asn^7 and Glu^{81} (Figure 2). Other aliphatic ^1H and ^{13}C resonances were assigned using the HBHA(CO)NH, HN(CA)HA, C(CO)NH, H(CCO)NH, ^1H-^{13}C CT-HSQC and HCCH-TOCSY spectra.

The spin systems of the aromatic side-chain proton resonances were initially identified with the conventional two-dimensional DQF-COSY and TOCSY spectra. The ^{15}N-filtered NOESY spectrum on ^{15}N-labeled protein in 90% H_2O/10% ^2H_2O provided the correlation between aromatic protons and aliphatic protons without overlap of the amide proton resonances, thus correlating the spin systems of aromatic protons with H^β resonances. These aro-

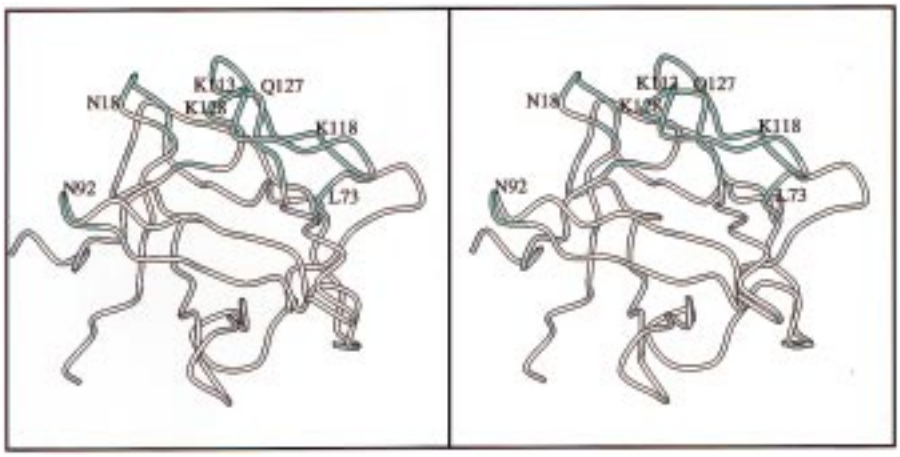

Figure 10. The location of the amino acid residues with chemical shift perturbation more than 50 Hz is plotted in stereo on the main-chain of the mean aFGF structure, where the side chain residues responsible for the heparin-hexasaccharide binding are also shown; Asn^{18}, Asn^{92}, Lys^{113}, Lys^{118}, Gln^{127}, Lys^{128}. These residues correspond to the counterparts which directly interact with the heparin-hexasaccharide in bFGF. The figure is prepared in quite similar orientation to Figure 3(b) of Faham et al. (1996), and was produced with the program MOLSCRIPT (Kraulis, 1991).

matic resonance assignments were confirmed by the three-dimensional ^{13}C-edited NOESY and the two-dimensional ^{1}H-^{13}C CT-HSQC spectra. The NH_2 groups of Gln and Asn residues were connected to their H^{β} and H^{α} protons with the three-dimensional ^{15}N-edited NOESY spectrum.

The main-chain and side-chain ^{1}H, ^{13}C and ^{15}N resonance assignments are summarized in the supplementary material. The backbone resonances were assigned for all residues and side-chain ^{1}H, ^{13}C, and ^{15}N resonances were assigned for 99% of all side-chain atoms. It should be emphasized that all the spectra were acquired in 90% H_2O/10% $^{2}H_2O$ solution, thus avoiding ambiguities in chemical shift values due to different solvent conditions.

Secondary structure of free aFGF

Once the sequential assignments were completed, NOE correlations from three-dimensional ^{15}N-edited NOESY and ^{13}C-edited NOESY spectra were analyzed to obtain interproton distance constraints. The analysis of sequential and medium-range NOEs are summarized in Figure 3. Qualitative amide-proton exchange rates were also measured using cross sections of amide proton-water exchange peaks taken from ^{15}N-edited NOESY at the F_1 chemical shift of the water (Pfuhl et al., 1995). Since this experiment was performed without solvent presaturation, the intensities of the amide proton-water exchange peaks can be qualitatively correlated with the exchange rates. Residues whose amide protons exchanged rapidly with solvent were identified by the presence of intense amide proton-water cross peaks. Since these exchange peaks developed within the 80 ms mixing time, the exchange rates of these amide protons were estimated to be on the order of 10 s^{-1}. Therefore, these residues are exposed to the surface and do not participate in stable hydrogen bonds. Dihedral angle constraints for backbone ϕ angles were determined from $^{3}J_{H}N_{H}\alpha$ coupling constants calculated from H^{α}/H^{N} intensity ratios in the 3D HNHA spectrum. Coupling constants greater than 8 Hz were used for dihedral angle constraints. Because the overlapped signals and the residues which have intermediate coupling constants were excluded, the total number of the dihedral angle constraints were 51 on the final stage of the structure calculation. From sequential NOE connectivities together with coupling constants and amide proton exchange information, the secondary structures of aFGF was identified (Figure 3). aFGF is a β-sheet rich protein containing eleven β-strands without α-helices. The Chemical shift index (CSI) of free aFGF was calculated for H^{α}, C^{α}, C^{β} and C' resonances (Wishart and Sykes, 1994) and its consensus was obtained. The consensus CSI (Figure 3) also indicated that aFGF consists of eleven β-strands connected by turns and had no apparent α-helices. Although the positions of the β-strands were shifted, truncated or elongated by one or two residues, the predicted secondary structure of aFGF from CSI was excellent agreement with the secondary structure obtained by present NMR experiments. The secondary

structure and β-sheet topology of free aFGF were subsequently derived from the information summarized in Figure 4 together with inter-strand NOEs. The triple-repeat of β-sheets is remarkable. According to the crystal structure (Zhu et al., 1991), aFGF consists of the following twelve β-strands; I (11–17), II (21–26), III (30–34), IV (42–48), V (53–59), VI (63–68), VII (72–76), VIII (83–89), IX (94–100), X (107–112), XI (116–120), and XII (130–136). The ranges of β-strands in the NMR structure are almost identical with the X-ray structure. However the residues 116–120 corresponding to β_{XI} do not have apparent evidence for β-strand formation in NMR structure. Thus, we concluded that aFGF consisted of eleven β-strands in solution; I (11–17), II (21–26), III (30–34), IV (43–48), V (53–58), VI (63–68), VII (72–76), VIII (84–89), IX (94–99), X (107–112) and XII (131–135) joined by turns (Figure 5). Moy et al. (1995) reported that bFGF also had no apparent β_{XI} from the analysis of the NOESY spectra. Thus, in solution, secondary structures of both aFGF and bFGF are quite similar with each other.

Tertiary structure of free aFGF

The remaining assignments of the three-dimensional ^{15}N-edited and ^{13}C-edited NOESY spectra were obtained using an in-house program for iterative cycles of NOESY assignments combined with structural calculations (Hatanaka et al., 1994). The structural calculations were based on 51 dihedral constraints and 1368 distance constraints which consist of 594 intraresidue and 774 interresidue containing 284 sequential ($|i - j| = 1$), 122 medium range ($2 \leq |i - j| \leq 5$), and 368 long range ($|i - j| > 5$) NOEs. A summary of the structural statistics for a set of the final structures and for the mean structure is shown in Table 2.

Figure 5 shows the overlay of the final 20 structures of aFGF obtained out of 200 runs of calculations (Figure 5a) and their mean structure (Figure 5b). In the solution structure, although β-strand regions were well converged, some loop regions were highly flexible. Figure 6 shows the number of distance constraints and the rmsd for the backbone atoms (N, C^{α}, C') for all residues. The residues in β-strand region have many long range constraints, and the rmsd values were 0.4–0.6 Å for the backbone atoms. On the other hand, the residues in the loop region have less long range constraints, and the rmsd values were more than 1.0 Å for the backbone atoms. Especially, two loop regions around Gly^{20} and Glu^{60} were extremely large rmsd values more than 1.5 Å. Overall estimated rmsd values of the 20 final structures from the minimized averaged structure were 0.58 ± 0.08 Å for the backbone atoms (N, C^{α}, C') and 1.09 ± 0.09 Å for the nonhydrogen atoms of residues 11–136 except for highly flexible loop regions of residues 17–20, 50–52, 59–62, 91–93, 100–106 and 113–130.

Figure 7 shows the Ramachandran plot for all residues in the minimized averaged solution structure of free aFGF. aFGF comprises 114 non-glycine and non-proline residues. The $\phi\psi$-plot indicates 60 residues (52.6%) in most favored regions, 44 residues (38.6%) in additional allowed regions, and 9 residues (7.9%) in generously allowed regions. Although Ser^{139} was in disallowed region, this residue is located on the C-terminal flexible tail. Figure 7 also shows the Ramachandran plots for four residues corresponding to β_{XI} identified in the X-ray crystal structure of aFGF (Zhu et al., 1991). Although the NOE-based analysis (Figure 3) showed that β_{XI} does not have apparent evidence for β-strand-formation (i.e. large H^N-H^{α} coupling constants, intense H^{α}(i) – H^N(i+1) NOE signals, and CSI), the ϕ and ψ maps for the solution and the crystalline structures of aFGF and the solution structure of bFGF supported that this region took β-strand-like structure.

Figure 8 shows an overlay plot of the crystal and solution structures of aFGF. The rmsd difference between the solution structure and the X-ray structure (Zhu et al., 1991) was 1.61 Å for the overall backbone atoms excluded highly flexible loop regions. aFGF takes a β-trefoil structure similar to the solution structure of bFGF and the crystal structures of aFGF and bFGF. The cavity in the center of the β-trefoil structure was surrounded by hydrophobic residues composed of Leu^{14}, Leu^{23}, Leu^{44}, Ile^{56}, Leu^{65}, Phe^{85}, Tyr^{97}, Val^{109} and Phe^{132} (Figure 5c), where the overlay of 20 structures of the side chains was shown on the main chain of aFGF. These residues were located with apparent three-fold axis symmetry. The central hydrophobic cavity is characteristic to the β-trefoil proteins and is found in the crystal structure of aFGF, bFGF and IL-1β (Zhu et al., 1991; Blaber et al., 1996). The corresponding hydrophobic residues are conserved or type-conserved in the FGF family proteins (Figure 1), suggesting that the hydrophobic interaction in the cavity plays an important role for maintaining the overall structure.

Binding site of heparin-derived hexasaccharide

To identify the heparin-binding site on aFGF, we studied the chemical shift perturbation of NMR resonances upon binding of heparin-derived hexasaccharide (Hep6). Hep6 is known to be a minimum aFGF binding unit without receptor activation. Upon addition of Hep6 to aFGF solution, the signal intensities of aFGF in ^{1}H-^{15}N HSQC spectrum were significantly reduced, suggesting that aFGF was oligomerized upon complex formation with Hep6. Oligomerization of heparin-binding proteins on the heparin chain is general characteristics (Spivak-Kroizman et al., 1994; Iwasaki et al., 1997). In the case of bFGF, Moy et al. (1997) reported that bFGF bound to heparin-tetrasaccharide in dimer with trans configuration and bound to decasaccharide in tetramer with trans and cis configurations. The sequential assignments of the back-bone resonances of the Hep6-aFGF complex were completed using the series of the triple resonance experiments (data not shown). Figure 9 shows the chemical shift perturbation of H^N, N, C′ and C^α resonances for each residue between free aFGF and the Hep6-aFGF complex. Because overall signals were extremely broadened in the Hep6-aFGF complex, we could not connect the main chain assignments to those of side chains. It should be noted that the residues with appreciable chemical shift perturbations in slow exchange condition were localized in some specific regions, supporting that aFGF did not show any significant overall conformation change upon complex formation. The main-chain amide proton resonance of Lys^{113} and the main-chain amide ^{15}N resonance of Lys^{118} were significantly perturbed by 0.72 ppm and 1.5 ppm, respectively. The following residues shifted more than 50 Hz in the sum of four (H^N, N, C′ and C^α) resonances upon Hep6-binding; Ser^{17}, Gly^{20}, His^{21}, Leu^{73}, Glu^{91}, Asn^{92}, Gly^{110}–Gly^{120}, Arg^{122}–Ala^{129} and Leu^{131}. Amide proton and nitrogen resonances of Lys^{128} were not identified in Hep6-aFGF sample possibly due to line broadening. These residues were plotted in cyan on the main chain of aFGF which were localized on the specific surface (Figure 10). Although the magnitude of the perturbation is not directly corresponding to the measure of interaction, we can expect that these residues are located in or in the vicinity of the contact region with Hep6. Extensive mutagenic studies for bFGF demonstrated that Asn^{27}, Arg^{120}, Lys^{125} and Gln^{134} are major residues responsible for heparin binding. Moreover, there is additional residues responsible for weak binding, comprising Lys^{26}, Arg^{81}, Lys^{119}, Thr^{121}, Gln^{123}, Lys^{129} and Lys^{135}. It should be noted that amino acid residues from Lys^{119} through Lys^{135} located in the C-terminal domain of bFGF collectively contribute nearly 80% of the binding free energy (Thompson et al., 1994). Recent X-ray crystal structure of bFGF complexed with heparin oligosaccharide (Faham et al., 1996) demonstrated that bFGF contained high affinity heparin binding site; Asn^{27}, Arg^{120}, Lys^{125} and Gln^{134} and low affinity heparin binding site; Lys^{26}, Asn^{101} and Lys^{135} (Table 1). The amino acid residues with appreciable chemical shift perturbations plotted on the main chain of aFGF structure (Figure 10) are in good agreement with those suggested by the bFGF mutagenic studies (Thompson et al., 1994) and revealed by the structure of bFGF-heparin oligosaccharide complex. On the main chain, we plotted the C^α location of Asn^{18}, Asn^{92}, Lys^{113}, Lys^{118}, Gln^{127} and Lys^{128} which are counterpart residues responsible for heparin binding in bFGF (Figure 10). The locations of these residues are quite similar to those in bFGF, suggesting that aFGF and bFGF recognize heparin hexasaccharide in a similar manner. It is to be noted that all these residues are located on the highly flexible regions (Figure 6) so that the side chains adapt their locations for proper bindings to heparin oligosaccharides. Although the β_{XI} strand (116–120) is absent in the solution structure of free aFGF, the C^α and C′ chemical shift values for 116–120 in the complex have a preference for β-strand formation. In the crystalline structure of the bFGF-heparin oligosaccharide complex, β_{XI} is formed and Lys^{125} located on β_{XI} can interact with a heparin sulfate group (Faham et al., 1996). Since Lys^{125} (Lys^{118} in aFGF) is responsible for high affinity binding to heparin, the β_{XI}-strand formation upon heparin binding may be crucial for exertion of the biological function of FGF family proteins.

During the final stage of the revision of this manuscript, the aFGF and heparin decasaccharide complex was reported (DiGabriele et al., 1998). The heparin-binding site of aFGF deduced from chemical shift perturbation is in good agreement with the result of the crystal structure.

References

Bax, A. and Pochapsky, S.S. (1992) *J. Magn. Reson.*, **99**, 638–643.
Bienkowski, M.J. and Conrad, H.E. (1985) *J. Biol. Chem.*, **260**, 356–365.
Blaber, M., DiSalvo, J. and Thomas, K.A. (1996) *Biochemistry*, **35**, 2086–2094.

Brünger, A.T. (1993) *X-PLOR Version 3.1: A System for X-Ray Crystallography and NMR*, Yale University Press, New Haven, CT.

Burgess, W.H. and Maciag, T. (1989) *Annu. Rev. Biochem.*, **58**, 575–606.

Cavanagh, J., Fairbrother, W.J., Palmer III, A.G. and Skelton, N.J. (1996) *Protein NMR Spectroscopy: Principles and Practice*, Academic Press, San Diego, CA.

Davidson, J.M., Klagsburn, M., Hill, K.E., Buckley, A., Sullivan, R., Brewer, P.S. and Woodward, S.C. (1985) *J. Cell Biol.*, **100**, 1219–1227.

Delaglio, F., Grzesiek, S., Vuister, G.W., Zhu, G., Pfeifer, J. and Bax, A. (1995) *J. Biomol. NMR*, **6**, 277–293.

DiGabriele, A.D., Lax, I., Chen, D.I., Svahn, C.M., Jaye, M., Schlessinger, J. and Hendrickson, W.A. (1998) *Nature*, **393**, 812–817.

Faham, S., Hileman, R.E., Fromm, J.R., Linhardt, R.J. and Rees, D.C. (1996) *Science*, **271**, 1116–1120.

Flaumenhaft, R., Moscatelli, D. and Rifkin, D.B. (1990) *J. Cell. Biol.*, **111**, 1651–1659.

Gospodarowicz, D. and Cheng, J. (1986) *J. Cell. Physiol.*, **128**, 475–484.

Gospodarowicz, D. (1987) *Methods Enzymol.*, **147**, 106–119.

Habuchi, H., Suzuki, S., Saito, T., Tamura, T., Harada, T., Yoshida, K. and Kimata, K. (1992) *Biochem. J.*, **285**, 805–813.

Hatanaka, H., Oka, M., Kohda, D., Tate, S., Suda, A., Tamiya, N. and Inagaki, F. (1994) *J. Mol. Biol.*, **240**, 155–166.

Iwasaki, W., Nagata, K., Hatanaka, H., Inui, T., Kimura, T., Muramatsu, T., Yoshida, K., Tasumi, M. and Inagaki, F. (1997) *EMBO J.*, **16**, 6936–6946.

Jaye, M., Burgess, W.H., Shaw, A.B. and Drohan, W.N. (1987) *J. Biol. Chem.*, **262**, 16612–16617.

Kay, L.E., Keifer, P. and Saarinen, T. (1992) *J. Am. Chem. Soc.*, **114**, 10663–10665.

Kraulis, P.J. (1991) *J. Appl. Crystallogr.*, **24**, 946–950.

Laskowski, R.A., Rullmann, J.A., MacArthur, M.W., Kaptein, R. and Thornton, J.M. (1996) *J. Biomol. NMR*, **8**, 477–486.

Lindhal, U., Lindholt, K., Spillmann, D. and Kjellen, L. (1994) *Thromb. Res.*, **75**, 1–32.

McGee, G.S., Davidson, J.M., Buckley, A., Sommer, A., Woodward, S.C., Aquino, A.M., Barbour, R. and Demetriou, A.A. (1988) *J. Surg. Res.*, **45**, 145–153.

Moy, F.J., Seddon, A.P., Campbell, E.B., Böhlen, P. and Powers, R. (1995) *J. Biomol. NMR*, **6**, 245–254.

Moy, F.J., Seddon, A.P., Bohlen, P. and Powers, R. (1996) *Biochemistry*, **35**, 13552–13561.

Moy, F.J., Safran, M., Seddon, A.P., Kitchen, D., Böhlen, P., Aviezer, D., Yayon, A. and Powers, R. (1997) *Biochemistry*, **36**, 4782–4791.

Nabel, E.G., Yang, Z-y., Plautz, G., Forough, R., Zhan, X., Haudenschild, C.C., Maciag, T. and Nabel, G.J. (1993) *Nature*, **362**, 844–846.

Ogura, K., Terasawa, H. and Inagaki, F. (1996a) *J. Biomol. NMR*, **8**, 492–498.

Ogura, K., Terasawa, H. and Inagaki, F. (1996b) *J. Magn. Reson.*, **B112**, 63–68.

O'Keefe, E.J., Chiu, M.L. and Payner, R.E., Jr. (1988) *J. Invest. Dermatol.*, **90**, 767–769.

Pfuhl, M., Gautel, M., Politou, A.S., Joseph, C. and Pastore, A. (1995) *J. Biomol. NMR*, **5**, 48–58.

Pineda-Lucena, A., Jiménez, M.A., Nieto, J.L., Santoro, J., Rico, M. and Giménez-Gallego, G. (1994) *J. Mol. Biol.*, **242**, 81–98.

Ruoslahti, E. and Yamaguchi, Y. (1991) *Cell*, **64**, 867–869.

Saksela, O., Moscatelli, D., Sommer, A. and Rifkin, D.B. (1988) *J. Cell. Biol.*, **107**, 743–751.

Shaka, A.J., Lee, C.J. and Pines, A. (1988) *J. Magn. Reson.*, **77**, 274–293.

Shipley, G.D., Keeble, W.W., Hendrickson, J.E., Coffey, R.J. Jr. and Pittelkow, M.R. (1989) *J. Cell. Physiol.*, **138**, 511–518.

Sommer, A. and Rifkin, D.B. (1989) *J. Cell Physiol.*, **138**, 215–220.

Spivak-Kroizman, T., Lemmon, M.A., Dikic, I., Ladbury, J.E., Pinchasi, D., Huang, J., Jaye, M., Crumley, G., Schlessinger, J. and Lax, I. (1994) *Cell*, **79**, 1015–1024.

Tate, S., Tate, N.U., Ravera, M.W., Jaye, M. and Inagaki, F. (1992) *FEBS Lett.*, **297**, 39–42.

Thompson, L.D., Pantoliano, M.W. and Springer, B.A. (1994) *Biochemistry*, **33**, 3831–3840.

Thunberg, L., Backstrom, G. and Lindhal, U. (1982) *Carbohydr. Res.*, **100**, 393–410.

Vuister, G.W. and Bax, A. (1993) *J. Am. Chem. Soc.*, **115**, 7772–7777.

Wishart, D.S. and Sykes, B.D. (1994) *J. Biomol. NMR*, **4**, 171–180.

Wüthrich, K. (1986) *NMR of Proteins and Nucleic Acids*, John Wiley, New York, NY.

Yayon, A., Klagsbrun, M., Esko, J.D., Leder, P. and Ornitz, D.M. (1991) *Cell*, **64**, 841–848.

Zhu, X., Komiya, H., Chirino, A., Faham, S., Fox, G.M., Arakawa, T., Hsu, B.T. and Rees, D.C. (1991) *Science*, **251**, 90–93.

Zhu, X., Hsu, B.T. and Rees, D.C. (1993) *Structure*, **1**, 27–34.